IN-64
186035
42 P

NASA Contractor Report 191506

ICASE Report No. 93-47

ICASE

20 Years of Excellence

HIGH ORDER HYBRID NUMERICAL SIMULATIONS OF TWO DIMENSIONAL DETONATION WAVES

Wei Cai

NASA Contract No. NAS1-19480
July 1993

Institute for Computer Applications in Science and Engineering
NASA Langley Research Center
Hampton, Virginia 23681-0001

Operated by the Universities Space Research Association

National Aeronautics and
Space Administration

Langley Research Center
Hampton, Virginia 23681-0001

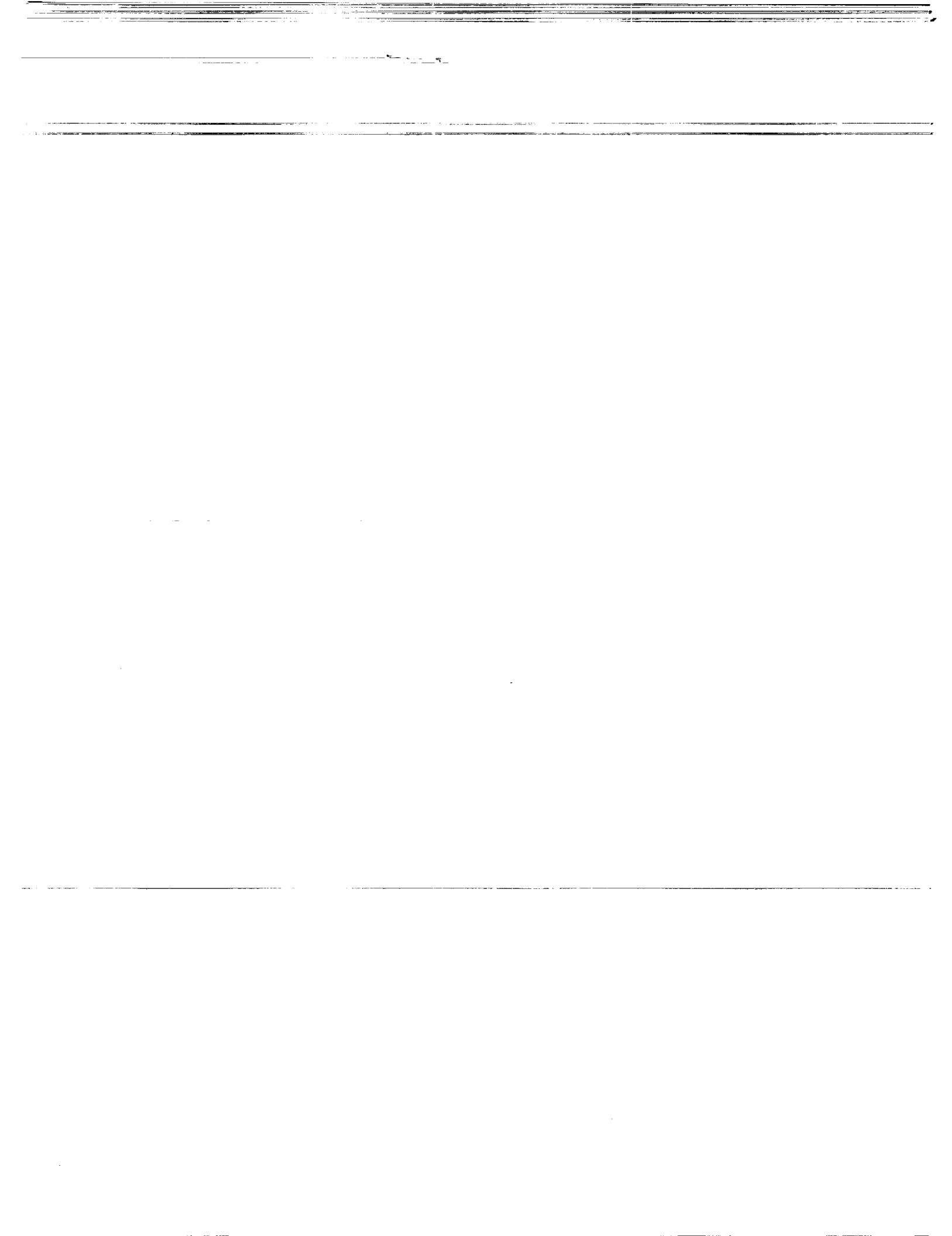

HIGH ORDER HYBRID NUMERICAL SIMULATIONS OF TWO DIMENSIONAL DETONATION WAVES

Wei Cai[1]

Department of Mathematics, University of North Carolina at Charlotte

ABSTRACT

In order to study multi-dimensional unstable detonation waves, we have developed a high order numerical scheme suitable for calculating the detailed transverse wave structures of multidimensional detonation waves. The numerical algorithm uses a multi-domain approach so different numerical techniques can be applied for different components of detonation waves. The detonation waves are assumed to undergo an irreversible, unimolecular reaction $A \rightarrow B$. Several cases of unstable two dimensional detonation waves are simulated and detailed transverse wave interactions are documented. The numerical results show the importance of resolving the detonation front without excessive numerical viscosity in order to obtain the correct cellular patterns.

[1]This work has been sponsored by NSF grant ASC-9113895 and is partially supported by the National Aeronautics and Space Administration under NASA contract NAS1-19480 while the auther was in residence at the Institute for Computer Applications in Science and Engineering (ICASE), NASA Langley Research Center, Hamption, VA 23681-0001. The computing facility was provided by a supercomputing grant from the North Carolina Supercomputer Center.

Introduction

Detonation waves are intrinsically multi-dimensional unstable phenomenon as demonstrated evidently by the experiments of Oppenheim [1] and White [2]. Since then, the simple steady Chapman-Jouquet theory [3], [4] has been re-examined for its limited explaination of most of the multi-dimensional features seen in real world detonation waves. The unique characteristic of multi-dimensional detonation waves are their cellular patterns which are the trajectories recorded on the wall by the transverse waves structures. Those transverse wave structures consist of so-called "triple points" which are of three shock configurations (an incident shock, a reflected shock and a Mach stem plus a contact discontinuity) [5]. The formation of those transverse wave structures moving along the main precursor detonation front attracted much attention. These phenomena raised the interest of experimentalists trying to measure the cell size of the cellular pattern [6].

There are many aspects in the investigations of detonation waves. Most important is the formation of a compressible detonation wave from laminar deflagration waves [7],[8] - a process called the DDT (Deflagration to Detonation Transition) process. In a DDT process, turbulent boundary layers are recognized as playing an important role in flame acceleration and the buildup of compressible pressure waves in front of flame fronts. The latter eventually will cause 'explosions in explosions' in the reacting flows and generate detonation waves. Applied mathematicians have made different attempts to identify the mechanism in the formation of triple points in the context of simplified mathematical models. In [9]-[11] Erpenbeck first used normal mode analysis on the linearized Euler system to study the stability of multi-dimensional detonation waves. Later, in [12], Strehlow introduced the concept of acoustic ray trapping to study the formation of Mach stems; this idea has been generalized by Majda [13] using high frequency asymptotics. With the rapid advent of modern computing capability, another available avenue in studying detonation phenomenon is by direct numerical simulations.

In this paper, we will present a high order hybrid method in order to study two dimen-

sional detonation waves, which will be able to resolve the detailed transverse wave structures of multi-dimensional detonation waves. The numerical simulations done in the paper are for an idealized model of chemical reaction in which the reactant species is in an irreversible, unimolecular reaction $A \rightarrow B$ with finite Arrhenius reaction rate. It is evident that this model can not represent all the effects of realistic chemical kinetics on the cellular structures observed in lab experiments. However, an accurate numerical solution of this simplified model will provide a better understanding of the physics involved in the onset and evolution of detonation waves and a verification of current mathematical theories on detonation waves.

There are three basic characteristics of detonation waves: (1) a strong precursor detonation front; (2) Mach stem configuration of the "triple points" and transverse wave structures; (3) stiff chemical reactions. The flow field can be divided into regions of highly irregular and steep gradients near the detonation front and regions of strong but smooth pressure waves. Near the shock fronts, strong vorticity fields are expected from the roll-up of slip lines. The temporal changes of thermodynamic and chemical compositions also vary dramatically from region to region. We will construct our numerical schemes according to these characteristics of multi-dimensional detonation waves, therefore , it is not surprising that the resulting numerical scheme is of a hybrid type.

The reaction rate depends on the flow temperature exponentially through the Arrhenius relation. Accurate computations of the flow field are extremely important in producing the correct chemical reactions and thus the correct cellular structures. Traditional shock capturing schemes, designed to smooth shock and contact discontinuities, introduce a considerable amount of numerical viscosity near those discontinuities. They have been shown to have a tendency to distort the real chemical reaction processes. In [14], the widely used P.P.M. high-order Godunov scheme was found to produce nonphysical weak detonations. Also in [15], the ENO finite difference scheme was shown to yield wrong detonation speeds in one dimensional ZND simulations. All these facts point out the importance of designing numerical methods without excessive numerical viscosity. Among the attemts of simulating two

dimensional detonation waves numerically, Oran et al has done a series of simulations with FCT schemes and a phenomenological chemistry model was used to solve the stiffness in the system, see for instance [16]. Another early result was obtained by Taki and Fujiwara [17] where a quasi first order numerical scheme was used with a two front model suggested in [18] to model the chemistry. Most recently, an improved version of P.P.M., which uses the location of the detonation in evaluating the numerical fluxes, gave improved results in one- and two-dimensional detonation simulations [19].

The work reported in this paper is part of a larger research project which intends to understand different aspects of detonation waves, including the DDT process and the effects of turbulence and the detonability and detonation failures. In Section 1, we will introduce the governing equations for reacting flows and its formulation in general curvilinear coordinates. In Section 2, we discuss the hybrid numerical scheme using multi-domain approaches, and the ENO finite difference methods and Chebyshev collocation methods and shock tracking methods will be introduced. These numerical techniques will be used in the framework of multi-domain to fit the properties of 2-D detonation waves. In Section 3, we consider the treatment of interface conditions between different numerical schemes and boundary conditions and the smoothing techniques for the detonation front. In Section 4, we validate the hybrid numerical scheme and test the effects of smoothing of the detonation front on the cellular pattern of detonation waves. Then, we present the main results of this paper, the simulations of several cases of two dimensional detonation waves. Detailed analysis of the results will be discussed. Finally, in Section 5 we give a conclusion and the plan for future works.

1 Governing Equations

Consider two dimensional detonation waves in an infinite channel moving from left to right into unreacted gas mixtures and the channel is denoted by Ω,

$$\Omega = (-\infty, \infty) X [-\frac{W}{2}, \frac{W}{2}] \tag{1}$$

where W is the channel width.

The governing equations for reacting detonation waves with s species and p reaction steps are the following Euler equations,

$$\frac{\partial \mathbf{u}}{\partial T} + \frac{\partial \mathbf{f(u)}}{\partial x} + \frac{\partial \mathbf{g(u)}}{\partial y} = \Phi(\mathbf{u}) \tag{2}$$

where

$$\mathbf{u} = (\rho, \rho u, \rho v, \rho e, \rho_1, \cdots, \rho_s)^{\mathsf{T}}$$

$$\begin{aligned}
\mathbf{f(u)} &= \left(\rho u, \rho u^2 + p, \rho uv, \rho u(e + \frac{p}{\rho}), \rho_1 u, \cdots, \rho_s u\right)^{\mathsf{T}} \\
\mathbf{g(u)} &= \left(\rho v, \rho vu, \rho v^2 + p, \rho v(e + \frac{p}{\rho}), \rho_1 v, \cdots, \rho_s v\right)^{\mathsf{T}} \\
\Phi(\mathbf{u}) &= (0, 0, 0, 0, \omega_1, \cdots, \omega_s)^{\mathsf{T}}
\end{aligned}$$

where $(u, v), \rho, p, e$ are velocity vector, density, pressure, and total specific internal energy. ρ_i is the mass density of the ith species. $\omega_i = \rho M_i \sum_{i=1}^{p} \nu_{ij} \frac{\partial \lambda_i}{\partial t}$ here M_i is the molecular weight of species -i and ν_{ij} is the stoichiometric coefficient for the $j-$species in the i-th reaction step, and $\frac{d\lambda_i}{dt}$ denotes the change rate of the ith reaction progress variable which is assumed to obey Arrhenius' rule. In the case of one-step $A \rightarrow B$ irreversible reaction, i.e. $s = p = 1$ and

$$\omega = -K\rho\lambda \exp(-\frac{E^+}{T}) \tag{3}$$

where $\lambda = \frac{\rho_1}{\rho}$ is the mass fraction of reactant. If we assume exthermoic reaction, the specific internal energy

$$e = \frac{p}{(\gamma - 1)\rho} + \frac{u^2 + v^2}{2} + \lambda Q \tag{4}$$

where Q is the specific heat formation and $\gamma = 1.2$ is the ratio of specific heats.

All quantities above have been non-dimensionalized by the initial states in the unreacted gas mixture in front of the detonation fronts. They are given as follows ("$\leftarrow$" indicates nondimensionalization and "0" subscript denotes states of unreacted gas)

$$\begin{array}{rcl} p & \leftarrow & \frac{p}{p_0} \\ \rho & \leftarrow & \frac{\rho}{\rho_0} \\ \mathbf{u} & \leftarrow & \frac{\mathbf{u}}{\sqrt{RT_0}} \\ T & \leftarrow & \frac{T}{T_0} \\ E^+ & \leftarrow & \frac{E^+}{RT_0} \\ Q & \leftarrow & \frac{Q}{RT_0} \\ t & \leftarrow & \frac{t}{t^*} \\ x & \leftarrow & \frac{x}{\ell^*} \end{array}$$

Where $t^* = \frac{\ell^*}{\sqrt{RT_0}}, \ell^* = x_{\frac{1}{2}}$ is the half reaction distance which a mass particle will travel from the detonation front before half-depletion of the reactant occurs.

Consider a general curvilinear coordinates $(\xi, \eta, t), \xi = \xi(x, y, T), \eta = \eta(x, y, T), t = t(x, y, T)$, the governing equation (2) becomes

$$\frac{\partial \mathbf{U}}{\partial \mathbf{t}} + \frac{\partial \mathbf{F(U)}}{\partial \xi} + \frac{\partial \mathbf{G(U)}}{\partial \eta} = \Psi(\mathbf{U}) \tag{5}$$

where $\mathbf{U} = \sqrt{\mathbf{g}}\mathbf{u}$,

$$\mathbf{F(U)} = \begin{pmatrix} U^1\sqrt{g}\rho \\ U^1\sqrt{g}\rho u + y_\eta p \\ U^1\sqrt{g}\rho v - x_\eta p \\ U^1\sqrt{g}\rho e + (y_\eta u - x_\eta v)p \\ U^1\sqrt{g}\rho_1 \\ \vdots \\ U^1\sqrt{g}\rho_s \end{pmatrix} \quad \mathbf{G(U)} = \begin{pmatrix} U^2\sqrt{g}\rho \\ U^2\sqrt{g}\rho u - y_\xi p \\ U^2\sqrt{g}\rho v + x_\xi p \\ U^2\sqrt{g}\rho e + (-y_\xi u + x_\xi v)p \\ U^2\sqrt{g}\rho_1 \\ \vdots \\ U^2\sqrt{g}\rho_s \end{pmatrix} \tag{6}$$

$$\Psi(\mathbf{U}) = (\mathbf{0}, \mathbf{0}, \mathbf{0}, \mathbf{0}, \sqrt{\mathbf{g}}\omega_1, \cdots, \sqrt{\mathbf{g}}\omega_s)^\top$$

where $\sqrt{g} = x_\xi y_\eta - x_\eta y_\xi$ is the Jacobian of the mesh transformation, $U^1 = \xi_t + u\xi_x + v\xi_y$, and $U^2 = \eta_t + u\eta_x + v\eta_y$. The spatial discretization is done in the (ξ, η) space for equation (5) and the range for ξ, η are both [-1,1].

In most of the numerical simulations done in the paper, for initial conditions we use the Chapman-Jouguet ZND steady solution which can be obtained by solving the Rankine-

Hugoit equation between the state in front of detonation front and all states behind the detonation front[5].

2 Hybrid Numerical Algorithm with Domain Decomposition Technique

In this section we describe the hybrid numerical scheme for detonation waves. The computational region is composed of the detonation front moving to the right and the rear piston boundary and upper and lower solid walls. It will be subdivided using multi-domain technique with the detonation front as the right most boundary (see Figure 1). Three different numerical techniques will be applied in different parts of the computational region. They are

- Shock tracking algorithm for the detonation front;
- High Order ENO finite difference scheme in the subdomain which contains the reflected shocks and contact discontinuities along the detonation front;
- Chebyshev collocation methods for the strong vorticity and pressure fields from the interaction of transverse waves along the detonation front.

We give a brief descriptions of each of the three numerical techniques.

2.1 Chebyshev collocation methods

In the computation domain $(\xi, \eta) \in [-1,1]X[-1,1]$, to approximate any quantity $f(\xi,\eta)$, we consider its Chebyshev collocation interpolant $I_N f(\xi,\eta)$ which is defined as (assuming that polynomials are of the same order N in both the ξ and η directions):

$$I_N f(\xi,\eta) = \sum_{0\le i,j\le N} f(\xi_i,\eta_j)\phi_i(\xi)\phi_j(\eta) \tag{7}$$

where $\phi_j(\xi) = \frac{(-1)^{j+1}(1-\xi^2)T'_N(\xi)}{\bar{c}_j N^2(\xi-\xi_j)}$, $\bar{c}_0 = \bar{c}_N = 2$ and $\bar{c}_j = 1$, for $1 \le j \le N-1$. Here $\xi_j = \cos\frac{j\pi}{N}$ are the Chebyshev-Gauss-Labotto points, and $T_N(\xi) = \cos(N\cos^{-1}(\xi))$ is the Chebyshev polynomial of the first kind.

The derivatives of $f(\xi,\eta)$ can be approximated by those of $I_N f(\xi,\eta)$, i.e.

$$\begin{aligned} f_\xi(\xi_k,\eta_l) \sim (I_N f)_\xi(\xi_k,\eta_l) &= \sum_{0\le i,j\le N} f(\xi_i,\eta_j)\phi_i'(\xi_k)\phi_j(\eta_l) \\ &= \sum_{0\le j\le N} \phi_j(\eta_l)[\sum_{0\le i\le N} f(\xi_i,\eta_j)\phi_i'(\xi_k)] \end{aligned} \tag{8}$$

where the inner summation in the square bracket can be evaluated either by matrix-vector-multiplication on a vectorized machine or by Fast Fourier Transformation. The latter method only involves $O(N^2 \log N)$ operations for the computation of all $f_\xi(\xi_k,\eta_l)$. Similar procedures can be obtained for $f_\eta(\xi_k,\eta_l)$.

2.2 High Order ENO Finite Difference Methods

To apply the ENO finite difference method to (5), the spatial derivative is discretized by conservative numerical flux differences:

$$\frac{\partial U_{i,j}}{\partial t} + \frac{\hat{F}_{i+\frac{1}{2},j} - \hat{F}_{i-\frac{1}{2},j}}{\Delta\xi} + \frac{\hat{G}_{i,j+\frac{1}{2}} - \hat{G}_{i,j-\frac{1}{2}}}{\Delta\eta} = \Psi(U_{i,j}) \tag{9}$$

where $U_{i,j}$ is the numerical approximation of (5) using the method of lines. In order to compute the numerical fluxes $\hat{F}_{i+\frac{1}{2},j}, \hat{G}_{i,j+\frac{1}{2}}$, first the primitive functions for $\mathbf{F},\mathbf{G}$ are approximated by piecewise polynomials using the ENO adaptive stencil idea of Harten [20],and then the derivatives of those polynomials are evaluated at the edge-centered mesh points $(\xi_{i+\frac{1}{2}},\eta_j),(\xi_i,\eta_{j+\frac{1}{2}})$ to produce the numerical fluxes. For technique details on the construction of ENO fluxes to the system of equations (5), we refer the reader to [20],[21].

We need the eigenvalues and eigenvector on the Jacobian of fluxes $\mathbf{A} = \frac{\partial \mathbf{F}}{\partial \mathbf{U}}, \mathbf{B} = \frac{\partial \mathbf{G}}{\partial \mathbf{U}}$ for the characteristic decompositions in order to define ENO numerical fluxes. If $\frac{D}{Dt} = \frac{\partial}{\partial t} + u\frac{\partial}{\partial x} + v\frac{\partial}{\partial y}$ denote the material derivative, then we have the following eigenvalues and eigenvectors,

Eigenvalues of **A**	Eigenvalues of **B**	Left Eigenvector of **A**	Right Eigenvector of **B**
$\frac{D\xi}{Dt} - \sqrt{(\xi_x^2 + \xi_y^2)}a$	$\frac{D\eta}{Dt} - \sqrt{(\eta_x^2 + \eta_y^2)}a$	$\mathbf{l}_1\mathbf{T}$	$\mathbf{T}^{-1}\mathbf{r}_1$
$\frac{D\xi}{Dt}$	$\frac{D\eta}{Dt}$	$\mathbf{l}_2\mathbf{T}$	$\mathbf{T}^{-1}\mathbf{r}_2$
$\frac{D\xi}{Dt}$	$\frac{D\eta}{Dt}$	$\mathbf{l}_3\mathbf{T}$	$\mathbf{T}^{-1}\mathbf{r}_3$
$\frac{D\xi}{Dt}$	$\frac{D\eta}{Dt}$	$\mathbf{l}_4\mathbf{T}$	$\mathbf{T}^{-1}\mathbf{r}_4$
$\frac{D\xi}{Dt} + \sqrt{(\xi_x^2 + \xi_y^2)}a$	$\frac{D\eta}{Dt} + \sqrt{(\eta_x^2 + \eta_y^2)}a$	$\mathbf{l}_4\mathbf{T}$	$\mathbf{T}^{-1}\mathbf{r}_4$

and

$$\begin{aligned}
\mathbf{l}_1 &= (1, -n_x\rho a, -n_y\rho a, 0, 0) & \mathbf{r}_1 &= \tfrac{1}{2}(1, -\tfrac{n_x}{\rho a}, -\tfrac{n_y}{\rho a}, \tfrac{1}{a^2}, 0)^\top \\
\mathbf{l}_2 &= (0, -n_y, n_x, 0, 0) & \mathbf{r}_2 &= (0, -n_y, n_x, 0, 0)^\top \\
\mathbf{l}_3 &= (1, 0, 0, -a^2, 0) & \mathbf{r}_3 &= (0, 0, 0, -\tfrac{1}{a^2}, 0)^\top \\
\mathbf{l}_4 &= (0, 0, 0, 0, 1) & \mathbf{r}_4 &= (0, 0, 0, 0, 1)^\top \\
\mathbf{l}_5 &= (1, n_x\rho a, n_y\rho a, 0, 0) & \mathbf{r}_5 &= \tfrac{1}{2}(1, \tfrac{n_x}{\rho a}, \tfrac{n_y}{\rho a}, \tfrac{1}{a^2}, 0)^\top
\end{aligned} \tag{10}$$

where $a = \sqrt{\frac{\gamma p}{\rho}}$ is the sound speed and $n_x = \frac{\xi_x}{\sqrt{\xi_x^2+\xi_y^2}}, n_y = \frac{\xi_y}{\sqrt{\xi_x^2+\xi_y^2}}$ for **A** and $n_x = \frac{\eta_x}{\sqrt{\eta_x^2+\eta_y^2}}, n_y = \frac{\eta_y}{\sqrt{\eta_x^2+\eta_y^2}}$ and the transform matrix $\mathbf{T} = \frac{\partial \mathbf{v}}{\partial \mathbf{u}}$ with $\mathbf{v} = (p, u, v, \rho, \lambda)$ being the primitive variable,

$$\mathbf{T} = \begin{pmatrix}
\frac{\gamma-1}{2}(u^2+v^2) & -(\gamma-1)u & -(\gamma-1)v & (\gamma-1) & -(\gamma-1)Q \\
-\frac{u}{\rho} & \frac{1}{\rho} & 0 & 0 & 0 \\
-\frac{v}{\rho} & 0 & \frac{1}{\rho} & 0 & 0 \\
1 & 0 & 0 & 0 & 0 \\
\frac{\lambda}{\rho} & 0 & 0 & 0 & \frac{1}{\rho}
\end{pmatrix} \tag{11}$$

2.3 Tracking Algorithm for Precursor Detonation Front

The detonation front will be represented by a continuous curve

$$x = x(y,t), \qquad \frac{-W}{2} \le y \le \frac{W}{2}, \; t \ge 0 \tag{12}$$

and the normal of the front denoted by $\mathbf{n} = (n_x, n_y)$ points to the unreacted gas, which can be computed by

$$\begin{aligned} n_x &= \frac{1}{\sqrt{1+(x_y)^2}} \\ n_y &= \frac{-x_y}{\sqrt{1+(x_y)^2}}. \end{aligned} \tag{13}$$

By the Hygen's principal, the detonation front will propagate in its normal direction with speed

$$D_n = \frac{x_t}{\sqrt{1+(x_y)^2}}. \tag{14}$$

Following the procedure proposed in [23] [22], we can write the Rankine-Hognoit condition across the shock front as follows

$$\begin{cases} \rho_0(u_{n,0} - D_n) &= \rho_1(u_{n,1} - D_n) \\ \rho_0(u_{n,0} - D_n)^2 + p_0 &= \rho_1(u_{n,1} - D_n)^2 + p_1 \\ \frac{\gamma}{\gamma-1}\frac{p_0}{\rho_0} + \frac{1}{2}(u_{n,0} - D_n)^2 + \lambda_0 Q &= \frac{\gamma}{\gamma-1}\frac{p_1}{\rho_1} + \frac{1}{2}(u_{n,1} - D_n)^2 + \lambda_1 Q \\ \rho_0\lambda_0(u_{n,0} - D_n) &= \rho_1\lambda_1(u_{n,1} - D_n) \end{cases} \tag{15}$$

where "0" denotes the state in front of detonation front and "1" the states behind the front. And $u_n = (u, v) \circ \mathbf{n}$ is the normal velocity on the front. Equation (15) relates the states in front of the shock and behind the shock. To close the system, we need to impose the continuity of tangential velocity, i.e.

$$u_{t,0} = u_{t,1}. \tag{16}$$

where $u_t = (-n_y, n_x) \circ (u, v)$ is the tangential velocity.

From (15) (16), we can solve the quantities $(p_1, \rho_1, u_{n,1}, u_{t,1}, \lambda_1)$ behind the shock in terms of those in front of the shock $(p_0, \rho_0, u_{n,0}, u_{t,0}, \lambda_0)$. Using the notation in [9], we have the following

$$\begin{aligned} \rho_1 &= \rho_0 \frac{(\gamma+1)\kappa^2}{(\gamma\kappa^2+1)(1-w)} \\ p_1 &= p_0 \frac{(\gamma\kappa^2+1)(1+w\gamma)}{\gamma+1} \\ u_{n,1} &= u_{n,0} - (u_{n,0} - D_n)(1 - \frac{\rho_0}{\rho_1}) \end{aligned} \tag{17}$$

$$
\begin{aligned}
u_{t,1} &= u_{t,0} \\
\lambda_1 &= \lambda_0
\end{aligned}
$$

where $w = \frac{\kappa^2-1}{\gamma\kappa^2+1}$ and $\kappa = \frac{|D_n - u_{n,0}|}{c_0}$ is the Mach number of the shock front relative to the unreacted gas and $c_0 = \sqrt{\frac{\gamma p_0}{\rho_0}} = \sqrt{\gamma}$ is the sound speed in the unreacted mixture.

In order to derive a time evolution equation for the shock front, we define the time differentiation along the shock front $\frac{d}{dt} = \frac{\partial}{\partial t} + x_t(y,t)\frac{\partial}{\partial x}$ for any fixed $y \in [-W/2, W/2]$. By applying $\frac{d}{dt}$ on both sides of (17) and separating the terms which involves $x_{tt}(y,t)$, we obtain the following

$$
\begin{aligned}
\frac{dp_1}{dt} &= c_1 x_{tt} + d_1 \\
\frac{d\rho_1}{dt} &= c_2 x_{tt} + d_2 \\
\frac{du_1}{dt} &= c_{3,u} x_{tt} + d_{3,u} \\
\frac{dv_1}{dt} &= c_{3,v} x_{tt} + d_{3,v} \\
\frac{d\lambda_1}{dt} &= c_4 x_{tt} + d_4
\end{aligned}
\tag{18}
$$

where

$$
\begin{aligned}
c_1 &= \frac{4\rho_0\tau}{(1+\gamma)(1+(x_y)^2)} \\
d_1 &= \frac{dp_0}{dt}\frac{2\gamma\kappa^2+1-\gamma}{1+\gamma} - \frac{2\rho_0}{(1+\gamma)(1+(x_y)^2)}[2\tau N_t + \kappa^2 S_t] \\
c_2 &= \frac{4(\gamma+1)\kappa^2}{\tau[(\gamma-1)\kappa^2+2]^2} \\
d_2 &= \frac{\rho_1}{\rho_0}\frac{d\rho_0}{dt} + \frac{2(\gamma+1)\rho_0\kappa^2}{[(\gamma-1)\kappa^2+2]^2}[\frac{2N_t}{\tau} - \frac{S_t}{S}] \\
c_{3,u} &= \frac{c_{3,n} + x_y c_{3,t}}{1+(x_y)^2} \\
d_{3,u} &= \frac{d_{3,n} + x_y d_{3,t}}{1+(x_y)^2} \\
c_{3,v} &= \frac{-x_y c_{3,n} + c_{3,t}}{1+(x_y)^2} \\
d_{3,v} &= \frac{-x_y d_{3,n} + d_{3,t}}{1+(x_y)^2}
\end{aligned}
$$

$$
\begin{aligned}
c_{3,n} &= \frac{2}{\gamma+1}(1+\frac{1}{\kappa^2}), \qquad c_{3,t}=0 \\
d_{3,n} &= x_{yt}v_1 + \frac{(\gamma-1)\kappa^2-2}{(\gamma+1)\kappa^2}N_t - \frac{2}{(\gamma+1)}\frac{S_t}{\tau}, \qquad g_{3,t} = T_t - x_{yt}u_1 \\
f_4 &= 0, \qquad g_4 = \frac{d\lambda_0}{dt}
\end{aligned}
$$

and $S=(1+(x_y)^2)c_0^2, N=u_0-x_yv_0, T=x_yu_0+v_0$ and $N_t=\frac{dN}{dt}, T_t=\frac{dT}{dt}, S_t=\frac{dS}{dt}$.

Using $\frac{d\mathbf{v}_1}{dt}=\frac{\partial \mathbf{v}}{\partial \mathbf{u}}\frac{d\mathbf{u}_1}{dt}=T\frac{d\mathbf{u}_1}{dt}$, equation (18) can be rewritten for conservative variable $\mathbf{u}$,

$$
T\frac{d\mathbf{u}_1}{dt} = T\mathbf{c}x_{tt} + T\mathbf{d} \tag{19}
$$

where $\mathbf{c}=(c_1,c_2,c_{3,u},c_{3,v},c_4)^\top, \mathbf{d}=(d_1,d_2,d_{3,u},d_{3,v},d_4)^\top$.

Now on a fixed point on the shock front we consider the characteristic component of equation (2) in the normal direction $\mathbf{n}=(\frac{1}{\sqrt{1+(x_y)^2}},\frac{-x_y}{\sqrt{1+(x_y)^2}})$,

$$
\frac{\partial \mathbf{u}}{\partial t} + \frac{\partial}{\partial \mathbf{n}}\tilde{\mathbf{f}} + \frac{\partial}{\partial \mathbf{t}}\tilde{\mathbf{g}} = \Phi. \tag{20}
$$

where $\mathbf{t}$ is the tangential direction along the shock front. $\tilde{\mathbf{f}}=n_x\mathbf{f}+n_y\mathbf{g}, \tilde{\mathbf{g}}=-n_y\mathbf{f}+n_x\mathbf{g}$. The eigenvalues and eigenvector of Jacobian matrix $\tilde{\mathbf{A}}=\frac{\partial \tilde{\mathbf{f}}}{\partial \mathbf{u}}$ are

$$
u_n-c, u_n, u_n, u_n, u_n+c \tag{21}
$$

$$
\mathbf{l}_1T, \mathbf{l}_2T, \cdots, \mathbf{l}_5T \tag{22}
$$

where $\mathbf{l}_i, i=1,\cdots,5$ are given in (10) with $n_x=\frac{1}{\sqrt{1+(x_y)^2}}, n_y=\frac{-x_y}{\sqrt{1+(x_y)^2}}$ and $u_n=n_xu+n_yv$.

Along the normal direction of the shock front, the (u_n+c)-characteristic field approaches the shock front from behind, therefore a compatibility condition can be obtained by considering the characteristic combination of equation (19)

$$
\mathbf{l}_5T\frac{d\mathbf{u}_1}{dt} = \mathbf{l}_5T\mathbf{c}x_{tt} + \mathbf{l}_5T\mathbf{d}, \tag{23}
$$

thus yielding the following ODE for the shock speed

$$
x_{tt} = H(\mathbf{u}_1, \mathbf{u}_0, x_y, x_t, x_{ty}) \tag{24}
$$

where

$$H = \frac{\mathbf{l}_5 T \frac{d\mathbf{u}_1}{dt} - \mathbf{l}_5 T \mathbf{d}}{\mathbf{l}_5 T \mathbf{c}}$$

and

$$\frac{d\mathbf{u}_1}{dt} = \mathbf{U}_1 \frac{\mathbf{d}}{\mathbf{dt}} \frac{\mathbf{1}}{\sqrt{\mathbf{g}}} + \frac{\mathbf{1}}{\sqrt{\mathbf{g}}} \frac{\partial \mathbf{U}_1}{\partial \mathbf{t}}$$

and $\frac{\partial \mathbf{U}_1}{\partial \mathbf{t}} = -\frac{\partial \mathbf{F}(\mathbf{U})}{\partial \xi} - \frac{\partial \mathbf{G}(\mathbf{U})}{\partial \eta} + \Psi(\mathbf{U})$ is the residual computed in (ξ, η) space behind the shock front.

3 Interface Conditions and Smoothing of Detonation Front

3.1 Interfacial Conditions between Subdomains and Boundary Conditions

We first discuss the issue of interface and boundary conditions for the hybrid numerical scheme. A correct interface coupling between the ENO finite difference method and spectral method is crucial for the global stability and accuracy of the scheme. The basic idea behind the treatment of interface and boundary condition is the propagation of information along characteristics of the hyperbolic systems [24]. We will consider the following situation separately.

Case 1. Interface between subdomains

On a typical interface between two subdomains, say Γ between Ω_l and Ω_r in Figure 1a, there are two types of points, i.e. interior point **I** and cross point **T**.

(a) Interior points **I**

Let $\mathbf{v} = (P, u, v, \rho, \lambda)^\top$ be the primitive flow variable, $\mathbf{v}^l, \mathbf{v}^r$ denote the solutions computed for the time step t^{n+1} in Ω_l, Ω_r. $S_{\Gamma,I}$ denotes the normal speed of the interface at point I with the normal direction $\mathbf{n} = (n_x, n_y)$. The eigenvalues and eigenvectors of the Jacobian matrix $\tilde{A}$ are given in (10) and (22), and the corresponding characteristic variables are

$$w_1 = p - \bar{a}\bar{\rho}u_n \tag{25}$$

$$w_2 = u_t \tag{26}$$

$$w_3 = p - \bar{a}^2\rho \tag{27}$$

$$w_4 = \lambda \tag{28}$$

$$w_5 = p + \bar{a}\bar{\rho}u_n \tag{29}$$

where "$\bar{\ }$" denotes an average state between $\mathbf{v}^l$ and $\mathbf{v}^r$, for instance the Roe-average [28].

In order to update $\mathbf{v}$ at point I for the time step t^{n+1}, we make the following correction on $w_i, 1 \le i \le 5$ based on the sign of the difference between the eigenvalues and the normal speed of the interface $S_{\Gamma,I}$, i.e.

$$w_i^{corrected} = \begin{cases} w_i^r & \text{if } \lambda_i - S_{\Gamma,I} < 0 \\ w_i^l & \text{if } \lambda_i - S_{\Gamma,I} \ge 0. \end{cases} \tag{30}$$

Finally, we set $\mathbf{v}^r = \mathbf{v}^l = \mathbf{v}^{corrected} = T^{-1}\mathbf{w}^{corrected}$.

Remark. In the case that the interface is the shock front, $\mathbf{v}^l$ should be computed by the Rankine-Hogoniot conditions (17).

(b) Cross points between the wall boundary and interior interface - "T" points

In order to update the solution for point "T" in Figure 1a we have to consider the information which comes from both subdomains Ω_l and Ω_r and also the role of the wall. Characteristic surfaces approaching the point "T" from several direction can be used to form a closed system to determine this solution [25] [26]. Thus, such an approach is not unique and based largely on the experience.

First let us consider the characteristic surface which is tangential to the interface Γ with normal $\mathbf{n} = (n_x, n_y) = (1, 0)$. The corrected characteristic quantities w_1, w_4, w_5 can be obtained as follows, assuming $\lambda_1, \lambda_4, \lambda_5$ all positive (otherwise, replace subscript "l" by "r" for each negative values of $\lambda_i - S_{\Gamma,T}, i = 1, 4, 5$),

$$w_1^x = w_1^{corrected} = p^l - \bar{a}\bar{\rho}u_n^l \tag{31}$$

$$w_4^x = w_4^{corrected} = \lambda^l \tag{32}$$

$$w_5^x = w_5^{corrected} = p^l + \bar{a}\bar{\rho}u_n^l. \tag{33}$$

where subscript "x" indicates the normal direction of the characteristic surface and $u_n = \mathbf{u} \circ \mathbf{n}$.

On the other hand, we know that the entropy s remains constant along the characteristic direction corresponding to the eigenvalue $u_n = \mathbf{u} \circ \mathbf{n}$, we can correct the entropy s as follows

$$s^{corrected} = \begin{cases} \frac{p^l}{(\rho^l)^\gamma} & \text{if } u_n - S_{\Gamma,T} > 0 \\ \frac{p^r}{(\rho^r)^\gamma} & \text{otherwise} \end{cases} \tag{34}$$

Next, we consider the characteristic surface approaching the wall at point "T" with normal $\mathbf{n} = (n_x, n_y) = (0, 1)$ - (top wall) or $(0, -1)$ - (lower wall). On the top wall, $u_n = v = 0$, so $\lambda_l = u_n - a = -a$ and we have the first characteristic field approaching the wall from the computational domain. Therefore, we can correct the first characteristic variable w_1^y using the results from either Ω_l or Ω_r, i.e.

$$w_1^y = w_1^{corrected} = \begin{cases} p^l + \bar{a}\bar{\rho}u_n^l & \text{if } u_n - S_{\Gamma,T} > 0 \\ p^r + \bar{a}\bar{\rho}u_n^r & \text{otherwise} \end{cases} \tag{35}$$

Finally, we solve for all four primitive quantities of the flow as follows

$$v = 0 \tag{36}$$

$$\lambda = w_4 \tag{37}$$

$$p = (w_1^x + w_5^x + 2w_1^y)/4 \tag{38}$$

$$\rho = (\frac{p}{s})^{\frac{1}{\gamma}}. \tag{39}$$

The treatment of the cross point on the lower wall can be done similarly.

Case 2. Wall Boundary Conditions

For a point on the wall which only belongs to one subdomain such as point "B" in Figure 1a, $\mathbf{n} = (n_x, n_y) = (0, 1)$ or $(0, -1)$ for top and lower walls, respectively. So $u_n = \mathbf{u} \circ \mathbf{n} = v = 0$, therefore the wall itself is a characteristic surface on which no normal flow condition is enforced, i.e. $v = 0$. Additionally, for the top wall (lower wall is treated similarly) we have the following compatibility equation according to its corresponding outflow characteristic field,

$$w_2 = -n_y u \tag{40}$$

$$w_3 = p - \bar{a}^2\rho \tag{41}$$

$$w_4 = \lambda \tag{42}$$

$$w_5 = p + \bar{a}\bar{\rho}u_n. \tag{43}$$

So, the solution at point "B" can be obtained as follows,

$$v = 0, u = -\frac{w_2}{n_y}, p = w_5, \lambda = w_4, \rho = (p^l - w_3)/\bar{a}^2. \tag{44}$$

3.2 Smoothing Technique of Detonation Front

In order to evolve the detonation front, we need to compute the time derivative of its normal speed D_n, which depends on x_{tt} in (24). Thus, the accuracy of the detonation front depends on the residual of numerical solution at the detonation front. Numerical experiments show that the front will develop high frequency numerical instability if no smoothing is applied on the detonation front. In this paper, we test three types of smoothing on the detonation front and compare the effects of different smoothing on the cellular pattern of detonation waves. Because detonation waves are unstable in most case in the high frequency range, this is a dilemma for our numerical simulation. On one hand, we try to admit as many frequencies in the numerical solution as possible in order to obtain enough nonlinear interaction between different unstable frequencies; on the other hand, to maintain numerical stability some cut-off in high frequencies is needed for long time integration. So, the best that we can hope for is to obtain as fine a resolution as possible in our numerical simulations while maintaining the numerical stability.

Smoothing Technique One - Averaging Solution on the Detonation Front

The simplest way to eliminate high frequency on the shock front is to smooth the solution $\mathbf{u}_1$ in $H(\mathbf{u}_1, \mathbf{u}_0, x_y, x_t, x_{ty})$ on the right hand side of (24).

Smoothing I. In equation (24) replacing $\mathbf{u}_{1,j}$ by the simple average of neighboring solutions,

which of course will reduce the accuracy of the solution on the detonation front,

$$\mathbf{u}_{1,j} \longleftarrow \frac{\mathbf{u}_{1,j-1} + 2\mathbf{u}_{1,j} + \mathbf{u}_{1,j+1}}{4}. \tag{45}$$

It can be seen that this averaging procedure will reduce the accuracy of the shock front to only first order, and have a larger dissipation than the other smoothing techniques suggested below.

Smoothing II - Derivative Smoothing

One of the most used methods in shock capturing scheme to control oscillations derivative limiting. The idea was first introduced in [27] to construct monotonicity preserving cubic spline.

Let $(x_i, y_i), i = 1, \cdots, n$ be n- discrete data points and $x_1 < x_2 \cdots < x_n$. The cubic spline $\Pi_3(x)$ is a piecewise cubic polynomial which has a continuous derivative at nodes x_i and satisfies the following conditions,

$$\begin{cases} \Pi_3(x_i) &= y_i \\ \Pi_3'(x_i) &= y_i' \end{cases} \qquad 1 \le i \le n. \tag{46}$$

and

$$y_i' = \frac{\Delta_{i-1} s_i + \Delta_{i-1} s_{i-1}}{\Delta_{i-1} + \Delta x_i} \qquad 2 \le i \le n-1$$

where $s_i = \frac{y_{i+1} - y_i}{\Delta x_i}, \Delta x_i = x_{i+1} - x_i$. The derivative at the end points is given by

$$\begin{aligned} y_1' &= \frac{(2\Delta_1 + \Delta_2)s_1 - \Delta_1 s_2}{\Delta x_1 + \Delta x_2} \\ y_n' &= \frac{(2\Delta_{n-1} + \Delta_{n-2})s_{n-1} - \Delta_{n-1} s_{n-2}}{\Delta x_{n-1} + \Delta x_{n-2}}. \end{aligned}$$

However, the cubic spline defined as above is usually oscillatory and the monotonicity of the original data set will be lost. It is suggested in [27] that the monotonicity can be preserved except at a local extrema point by limiting the derivatives y_i''s,

$$y_i' \longleftarrow y_{lim,i}' = \begin{cases} min(max(0, y_i'), 3min(s_{i-1}, s_i)) & \text{if } y_i' > 0 \\ max(min(0, y_i'), -3min(s_{i-1}, s_i)) & \text{if } y_i' \le 0. \end{cases} \tag{47}$$

So we suggest the following smoothing procedure for the detonation front,

SMOOTHING II. In equation (24) change x'_y in H as follows,

$$(x'_y)_i \longleftarrow (x'_y)_{lim,i}, \qquad 1 \leq i \leq n. \tag{48}$$

Smoothing Technique III - High Frequency Spectral Space Smoothing

The third smoothing technique tested in this paper applies high frequency cut-off functions in the Fourier transform space of the detonation front. Assume that the discrete data $x_i, 1 \leq i \leq n$ are equally distributed and data (x_i, y_i) has been decomposed into Fourier modes,

$$y_i = \sum_{k=-\frac{n}{2}}^{\frac{n}{2}-1} \hat{y}_k e^{ikx_i} \qquad 1 \leq i \leq n \tag{49}$$

where $\hat{y}_k = \frac{1}{n}\sum_{i=1}^{n} y_i e^{-ikx_i}$.

We multiply the Fourier coefficient $\hat{y}_k$ by a decreasing factor σ_k so that the high frequencies will be decreased. The modified y_i is given by

$$y_i \leftarrow (y_i)^{filtered} =: \sum_{k=-\frac{n}{2}}^{\frac{n}{2}-1} \sigma_k \hat{y}_k e^{ikx_i} \qquad 1 \leq i \leq n. \tag{50}$$

Here we chose σ_k so that it decays exponentially in terms of the wave number,

$$\sigma_k = e^{-\mu(\frac{2k}{n})^{2\ell}} \qquad \text{for } |k| \leq \frac{n}{2}, \tag{51}$$

where the constant μ is chosen so that $\sigma_{\frac{n}{2}}$ is the machine zero and 2ℓ is called the order of the exponential filtering.

4 Cellular Structures of Two Dimensional Detonation Waves

4.1 Linear Stability Analysis and 2 D Detonation Waves

In [9]-[11] Erpenbeck first used linearized normal mode analysis to study the stability of two dimensional detonation wave. With complex analysis technique, he analyzed the unstable modes of linearized Euler equations with respect to the steady state solution of plane ZND

detonation waves. The stability of the detonation front $\psi(y,z,t)$, thus the whole flow field, is determined by the existence of poles of its time Laplace transformation $\eta(\tau,\epsilon)$ for any transverse frequency $\epsilon = \alpha^2+\beta^2$. It is found that, for large wave numbers (high frequencies), the stability of ZND detonation waves depends on the quantity $c_0^2(x)-u^2(x)$ where x is the distance measured away from the ZND steady shock front and $c_0(x)$ is the frozen sound speed at location x and $u(x)$ is the flow velocity there. Detonation waves with an one step irreversible $A \rightarrow B$ reaction have been categorized [11] in terms of their short wave stabilities:

Type D $c_0^2(x)-u^2(x)$ is decreasing as x moves away from the detonation front;

Type I $c_0^2(x)-u^2(x)$ is increasing as x moves away from the detonation front;

Type M $c_0^2(x)-u^2(x)$ achieves a maximum at some points x^* between $x=0$ and $x=-\infty$.

Type D has been shown to be stable for high frequencies, while Type I and M will be unstable for bands of large wavenumbers, $\epsilon_{i,l} \leq \epsilon \leq \epsilon_{i,r}, i = 1,2,\cdots$ where $\epsilon = \frac{n\pi}{W}$ and W is the channel width. The latter case means difficulty in attempting to simulate detonation waves through numerical calculations as it will never be possible to resolve all the unstable modes in the system with finite a number of mesh points.

4.2 Validation of Numerical Scheme

Computational Mesh Set-up and Initial Conditions

The following notation will be used in all the computations: ndm - the number of subdomains in the subdivision of the computation domains; W - channel width; lsk - number of marker points on the shock front; (n,m) - size of mesh in a subdomain. In all the computations presented here, we take $ndm = 9$ and the total length of the channel to be $150\ell^*$ with the detonation front as the right boundary of the solution domain. As the detonation propagates and curves, the interfaces between subdomains will also travel at a speed which is taken to be the averaged speed of the curved detonation front.

In the first subdomain, we use third order ENO-LF schemes[21] in order to resolve the

reflected shocks and contact discontinuities. A stretching function will be used in the x-direction so that the mesh will be clustered toward the detonation front. The stretching function is given by

$$\xi^* = \psi(\xi) = -1 + \frac{2}{\alpha} \sin \frac{\sin^{-1} \alpha(\xi + 1)}{2} \qquad -1 \leq \xi, \xi^* \leq 1$$

where ξ^* is the stretched mesh and the parameter α determines the amount of stretching, we take $\alpha = 0.995$.

The right hand side of the first subdomain, being the detonation front, will be tracked by the track algorithm in Section 2.3. Appropriate smoothing will be applied on the detonation front for about every 20 iterations; the exact frequency depends on the strength of the detonation waves. Chebyshev collocation methods will be used in the remaining subdomains. In order to ease the CFL restriction from the nonuniform distribution of Chebyshev collocation points, another stretching function $\phi(x, \alpha)$ is used to produce a more uniformly distributed mesh in the Chebyshev collocation subdomains. We take

$$\xi^* = \phi(\xi) = \frac{\sin^{-1} \alpha\xi}{\sin^{-1} \alpha}$$

where again ξ^* is the stretched mesh and $\alpha = 0.999$ so that Chebyshev-Gauss-Labotto points in ξ space will be mapped to ξ^* space with more uniform distribution.

Finer meshes will be used for those subdomains closer to the denotation front. A typical mesh set-up is given in Figure 1b (only the first seven subdomains are shown).

The computation starts with the ZND steady state solution of plane detonation wave. To induce the transverse waves, we introduce perturbations either in the detonation front or in the flow variables themselves, or both. The type of perturbations used will be sine-like wave

$$x(y, 0) =: x(y, 0) + \epsilon \sin(\pi y^2), \qquad -W/2 \leq y \leq W/2 \tag{52}$$

or random perturbations ($\epsilon ranf()$).

Reflective solid boundary condition will be used in all computations.

Effect of Smoothing of the Detonation Front on the Cellular Patterns

The procedure of smoothing on the detonation front basically introduces extra numerical viscosity in the whole scheme, therefore the smaller this extra viscosity is, the more reliable the numerical simulations should be. This argument can be extended to any numerical simulation of detonation waves. To evaluate the effects of smoothing of the detonation front on the cellular structure, we consider the ZND detonation wave with heat formation $Q = 50$, activation energy $E = 50$, and the overdrive $f = 1.6$. The channel width is taken to be $W = 20\ell^*$. As we are not interested in the detailed structure of the flow field, we take a less fine mesh - $\sum_{i=1}^{9}(n,m) = (50,50)+(24,50)+(20,50)+(20,50)+(20,40)+(10,20)+(10,10)+(10,10)+(10,10)$. The number of marker points on the detonation front is $lsk = 160$. The initial size of the subdomains will be $5\ell^* \times W, 5\ell^* \times W, 5\ell^* \times W, 5\ell^* \times W, 10\ell^* \times W, 15\ell^* \times W, 25\ell^* \times W, 40\ell^* \times W, 40\ell^* \times W$. Three tests are done to see the effects of smoothing on the cellular pattern. In all the numerical results reported in this paper, the detonation front has traveled at least 20 channel width for the cellular patterns reported.

Test One Smooth I, II, and III

In the first test we activate all three types of smoothing on the detonation front. Thus, strong numerical viscosity will be produced to stablize the front. But, keep in mind, even in this situation, we still track the detonation front and no difference across the front is used in the scheme. In Figure 2a, we record the pressure on the detonation front for time $t = 10t^* - 20t^*$. A very regular and symmetric two cell structure is produced by the interaction of four different triple points. This correspond to a cell width $10\ell^*$ - half the channel width.

Test Two. Smooth II and III

In the second test, we deactivated Smooth I which produces the largest numerical viscosity among all three types of smoothing. In this case, only one cell is present in the cellular pattern (Fig 2b) which corresponds to a cell width $20\ell^*$.

Test Three Smooth III only

In the third test, we use only Smoothing III which uses high frequency attenuation in the Fourier transformation space for the shock front. The order of exponential cut-off in (51) is 12, thus yielding very slight numerical viscosity on the detonation front. The cellular pattern of the detonation front (Fig 2c) consists of two quite irregular cells, a larger cell and a smaller cell. Two major triple points dominate the cellular structure along with two secondary triple points. A close-up picture of the cell pattern is given in Fig 6a where we will further examine this case in more detail.

These tests show us the sensitivity of the cellular patterns of the detonation waves to the amount of numerical viscosity in the scheme. Consequently, we have to be very careful in applying the right kind of algorithm for the simulations if we want to compare the numerical results with either theoretical predictions or experiment results. Presumably, less numerical viscosity will produce more reliable cellular patterns. From this point on, all numerical results presented will use only the Smooth III procedure (about every 20 iterations), which has the smallest amount numerical viscosity, in order to stabilize the evolution of the detonation front. There have been several situations which demonstrate that such smoothing is necessary or the computation will abort prematurely.

Accuracy of Time Integration and Mesh Convergence Studies

1) Comparison of Time Discretizations

The stiffness in a chemically reacting system poses a lot of difficulty for numerical simulations. There are basically two issues to be considered when choosing a time integrator , one is accuracy and another is CPU time efficiency. For the one reaction system tested here, we could us either a time splitting method as in [19] [16] or just an explicit Runge-Kutta type method. For the splitting method, the evolution of the solution can be split into two steps, the first step being an Euler step where the governing equation is solved without the chemical reaction production terms; the second step involves only the reaction term with the temperature field frozen at the value of the previous Euler step. The second step can be

explicitly solved here because only one reaction is considered. However, if more complicated chemistry is involved, such splitting will not avoid the stiffness problem in the simulation.

We compare the results of the splitting method (which is at most second order) and the third order Runge-kutta method with the same resolution and spatial discretizations in the spatial directions. The detonation parameters are $Q = 50, E = 50, f = 3$; the mesh sizes are $\sum_{i=1}^{9}(n,m) = (100,100) + (34,70) + (20,40) + (20,40) + (20,30) + (10,20) + (10,10) + (10,10) + (10,10)$; and the channel width $W = 10\ell^*$. The initial size of the subdomains will be $5\ell^* \times W, 5\ell^* \times W, 5\ell^* \times W, 5\ell^* \times W, 10\ell^* \times W, 15\ell^* \times W, 25\ell^* \times W, 40\ell^* \times W, 40\ell^* \times W$. In Figure 3, we plot the pressure along the center of the channel at time $T = 34t^*$. The solid line is the result obtained by the third order Runge-Kutta method while the dots (o) are the results by the splitting method. We can see both results agree fairly well in most parts of the domain except that the splitting method fails to resolve the dip in the pressure. In the numerical tests given later, the third order Runge-Kutta method will be used in all the computations.

2) Mesh Convergence Studies

We use the same detonation parameter as above but with three different meshes in the spatial direction. the third order Runge-Kutta method is used in both cases. Mesh A is $\sum_{i=1}^{9}(n,m) = (100,100) + (34,70) + (20,40) + (20,40) + (20,30) + (10,20) + (10,10) + (10,10) + (10,10)$. Mesh B is $\sum_{i=1}^{9}(n,m) = (120,150) + (34,70) + (20,40) + (20,40) + (20,30) + (10,20) + (10,10) + (10,10) + (10,10)$. Mesh B is $\sum_{i=1}^{9}(n,m) = (160,200) + (34,70) + (20,40) + (20,40) + (20,30) + (10,20) + (10,10) + (10,10) + (10,10)$. The initial size of the subdomains will be $8\ell^* \times W, 5\ell^* \times W, 5\ell^* \times W, 5\ell^* \times W, 10\ell^* \times W, 12\ell^* \times W, 25\ell^* \times W, 40\ell^* \times W, 40\ell^* \times W$. So in the first subdomain, mesh A is about 10 points per ℓ^* and mesh B is about 15 points per ℓ^* and Mesh C is about 20 points per ℓ^*. In Figure 4, we plot the pressure along the center of the channel ((-) Mesh C, (o) Mesh B, (+) Mesh A). Close agreement can be seen among the results for all meshes. In the rest of the computation, we will use at least the resolution of Mesh B, which is about 15 points per half reaction distance.

4.3 Numerical Simulation of 2-D detonation Waves

We present four cases of detonation waves using our high order hybrid scheme, each belonging to one of the three types of detonations in terms of the short wave instability.

CASE I $Q = 10, E = 50, f = 1.2$, channel width $W = 10\ell^*$ - One cell pattern

This is a case of Type M detonation which is unstable for high frequencies. The mesh used in this case is $\sum_{i=1}^{9}(n,m) = (110,140) + (20,40) + (20,40) + (20,30) + (20,30) + (10,20) + (10,10) + (10,10) + (10,10)$. The number of "Marker Points" on the shock front is $lsk = 300$. The initial size of the subdomains will be $5\ell^* \times W, 5\ell^* \times W, 5\ell^* \times W, 5\ell^* \times W, 10\ell^* \times W, 15\ell^* \times W, 25\ell^* \times W, 40\ell^* \times W, 40\ell^* \times W$. This mesh gives a resolution of 14 points per half reaction distance in the ENO domain. As a result of the high accuracy of the Chebyshev collocation method, we find that very good resolution of the flow field can be obtained with far less points. We start the computation with the ZND steady state solution with a sine-like perturbation (52) on the shock front with $\epsilon = 0.15$.

In Figure 5a, we record the pressure along the shock front for time $t = 10t^* - 20t^*$. Only one cell is produced in this run which corresponds to two triple points along the detonation front. In Figure 5b, we contour five snapshots of the pressure, temperature, vorticity and mass fraction at time $T = 30.5t^*, 31.5t^*, 32.5t^*, 33.5t^*, 34.5t^*$. In Figure 5c, we sketch the interaction of the triple points which will be typical for all the other later cases. We can see the evolution of the reflected shock from the pressure field; the contact discontinuity can be best seen from the vorticity field. Because the contour lines hardly distinguish the exact position of contact lines, we can use the temperature field to locate the position of the curving contact lines. In the first time snapshot ($T = 30.5t^*$) of both Figure 5b and 5c, we see two reflected shocks (RS) A, B waves moving toward the center of the channel and to collide. Following RS - A, B are two contact discontinuities C_1^-, C_1^+ respectively, where the signs indicate opposite circulation of these two contact lines which produce opposite vorticities. In snapshot two ($T = 31.5t^*$), reflected shock A, B have emerged from the interaction,exchanged directions, and are moving away from each other. Notice that in

the field of mass fraction, the layer of unreacted gas is much thicker behind the incident shock than the one behind the Mach Stem. The chemical reaction in the layer behind the incident shock waves provide the energy for further development of reflected shocks A, B. The contact discontinuities C_1^-, C_1^+ are now detached from their triple point configurations, moving downstream, and their tips are rolled up. At the same time a new pair of contact lines C_2^+, C_2^- emerge behind the reflected shock waves B, A respectively. In snapshot three ($T = 32.5t^*$), RS - B, A are moving toward upper and lower wall respectively and are ready to be reflected away from the wall with the contact lines C_2^+, C_2^- following them. In snapshot three ($T = 33.5t^*$), RS B, A have been reflected away from the walls and the contact lines C_2^+, C_2^- detached from the triple point configuration while an another new pair of contact lines C_3^-, C_3^+ are created behind B and A respectively. In the last snapshot ($T = 34.5t^*$), RS - B, A are ready to collide again which finishes one cycle of the interaction of these two triple points.

Case II $Q = 50, E = 50, f = 1.6$, channel width $W = 20\ell^*$. Two cells pattern

This is a type M detonation wave which is unstable for high frequencies, and we use the mesh $\sum_{i=1}^{9}(n,m) = (50,250) + (34,70) + (20,40) + (20,30) + (20,30) + (10,20) + (10,10) + (10,10) + (10,10)$. The number of 'Marker Points' on the shock front is $lsk = 300$. Figure 6a shows a two cell pattern produced by the trajectories of four triple points. There is a larger cell with width approximately $10\ell^*$ (half the channel width) and a smaller one with width $5\ell^*$. Figure 6b contains six snapshots of the detonation at time $T = 20.25t^*, 21.5t^*, 22t^*, 22.5t^*, 23t^*, 23.5t^*$. The times were chosen so that the interaction of the triple points can be shown clearly in the contour plots. A random perturbation with magnitude $\epsilon = 0.3$ is used to perturb the shock front at $T = 0$. Four triple points are produced (two major ones and two secondary ones) and the cell pattern is given in Figure 6a. Referring to the six arrows and depicted shock fronts in the sketch Figure 6c which corresponds roughly the six time snapshots in Figure 6b . In the first time snapshot $T = 20.25t^*$, in the lower middle part of the channel, two triple points C, D are moving away from each

other just after collision and A has been reflected from the upper wall and is about to collide with triple point B. In snapshot two ($T = 21.5t^*$), in the upper part of the channel, two smaller triple points A, B collide and separate and, in the middle part of the channel triple point C is moving upward to collide with triple point A. Near the lower wall, triple point D is reflecting away from the lower wall. In snapshot three ($T = 22t^*$), triple point B is approaching the upper wall, triple points A and C collide, and triple point D keeps moving up away from the lower wall. In snapshot four ($T = 22.5t^*$), triple point B reflects away from the upper wall and is about to collide with triple point C, while triple points A and D are about to collide with each other. In snapshot five ($T = 23t^*$), in the upper part of the channel, triple points B and C collide and triple points A and D approach each other. Finally, in snapshot six ($T = 23.5t^*$), triple points B and C finish the collision and exchange directions while triple points A and D collide.

Also notice that in Snapshots 4 and 5, the two pressure waves from the reflected shocks intersect with each other before the collision of the triple points happens along the detonation front (Snapshot 6). Such interaction will cause sudden reaction of any unreacted gas in the interior region and produce so-called "explosions in explosions'.

Case III $Q = 50, E = 50, f = 3$, channel width $W = 10\ell^*$. One cell pattern and chaotic flow fields.

This case represents strong heat release, large overdrive, and belongs to type I which is again unstable for a range of high frequencies. We use a mesh $\sum_{i=1}^{9}(n,m) = (120,150) + (34,70) + (20,40) + (20,30) + (20,30) + (10,20) + (10,10) + (10,10) + (10,10)$; and the number of 'Marker points' on the shock front is $lsk = 300$. The initial size of the subdomains will be $5\ell^* \times W, 5\ell^* \times W, 8\ell^* \times W, 5\ell^* \times W, 10\ell^* \times W, 12\ell^* \times W, 25\ell^* \times W, 40\ell^* \times W, 40\ell^* \times W$. Only two triple points are produced in this case; an one cell pattern of the detonation front is given in Figure 7(a). In Figure 7(b), we have six time snapshots of the pressure, temperature, vorticity and mass fraction. Large vorticities are generated behind the detonation front and the flow field becomes quite chaotic. There are only two triple points along the detonation

front which produce a one cell pattern for the cellular structure with cell size $W = 10\ell^*$ (see Figure 7a).

5 Conclusion

We have developed a high order numerical scheme which is suitable for computing detailed transverse wave structures of two dimensional detonation waves. The numerical algorithm uses a multi-domain approach so that different numerical techniques can be applied for different components of detonation waves. The propagation of waves across the interfaces of subdomains have been very smooth and the order of accuracy of the whole numerical scheme is only limited by the accuracy of the time integrator. Tracking of the detonation front avoids differences across the detonation front, thus avoiding excessive numerical viscosity in shock capturing schemes. The high resolution of the Chebyshev collocation method enables us to use far less grid points in most of the solution domain and yields great savings in the total CPU cost. The potential for using higher ENO finite difference schemes in the subdomain which contains the reflected shocks and contact discontinuities can be further exploited.

We have shown that the cellular pattern of the detonation waves is affected by the accuracy of the detonation front and the amount of numerical viscosity, especially the amount of viscosity involved in the time evolution of the detonation front by the numerical scheme. We believe that this point should be well taken in the further investigation of detonation waves in order to have meaningful comparisons with experiment results.

We have studied several cases of detonation waves with specific ratio $\gamma = 1.2$, from small heat release (Case I) to large release (Case II and III) and small overdrives (Case I) to large overdrives (Case II, III). The numerical results successfully reproduced the onset and evolution of the transverse wave structures. The contact lines within triple points create large vorticity fields behind the detonation front which will distort and interact with the detonation front. The contact discontinuities from the triple points after their collisions convect downstream and generate vorticity downstream. Further work will be done by using

more realistic chemistry models so that comparison with experiment results will be possible.

Acknowledgement

The author would like to thank Prof. Youlan Zhu for his help in developing the shock tracking algorithms.

References

[1] Urtiew, P. A., Oppenheim, A. K. 1966. *Proc. Roy. Soc. London Ser. A* 295:13-28.

[2] White, D. R. 1961, *Phys. Fluids* 4:465-80.

[3] Berthelot, M., Vieeille, P. 1882. *C. R. Acad. Sci. Paris.* 94:101-8, seance du 16 Janvier, 1882; pp. 822-23, seance du 27 Mars, 1882; 95:151-57, seance du 24 juillet, 1882

[4] Chapman, W. R. and Wheeler, R. V., "The Propagation of Flames in Mixtures of Methane-air," Part IV. *J. Chem. Soc.* **1926**, 2139.

[5] Fickett, W. and Davis, W. C., *Detonation,* Unif. of California Press, 1979.

[6] Strehlow, R. A., *Combustion Fundamentals*, New York: McGraw-Hill Book Company, 1984.

[7] Shchelkin, K. I., Effect of Roughness of the Surface in a Tube on Origination and Propagation of Detonation in Gas. *J. of Exp. and Theo. Phys.* (U.S.S.R.) **10**, (1940), 823.

[8] Lee, J. H. S., Moen, I. O. 1980. "The mechanism of Transition from Deflagration to Detonation in Vapor Cloud Explosions," *Prog. Energy Combust. Sci.* 6:359-89

[9] Erpenbeck, J., "Stability of Idealized One-Reaction Detonations," *Phys. Fluids* **7**, 684–696, (1964).

[10] Erpenbeck, J., "Detonation Stability for Disturbances of Small Transverse Wavelength", *Phys. Fluids* **9** , 1293–1306, (1966).

[11] Erpenbeck, J., "Nonlinear Theory of Unstable Two-Dimensional Detonation," *Phys. Fluids* **13**, 2007–2026, (1970).

[12] Strehlow, R. A., Maurer, R. E., Rajan, S., "Transverse Waves in Detonations: I Spacing in the Hydrogen-Oxygen System," *AIAA J.* **7** (1969), 323-328.

[13] Majda, A. "Criteria for Regular Spacing of Reacting Mach Stems", *Proc. Natl. Acad. Sci. USA* 84:6011-6014 (1987).

[14] Colella, P., Majda, A., and Roytburd, V., "Theoretical and Numerical Structure for Reacting Shock Waves," *SIAM J. Sci. Stat. Computing* **4** (1986) 1059–1080.

[15] Engquist, B. E. and Sjogreen, B., "Robust Difference Approximations of Stiff Inviscid Detonation Waves," *UCLA CAM REPORT* 91-03 (1991).

[16] Oran, E. S, Boris, J. P., Flanigan. M., Burks, T., and Picone, M., "Numerical Simulations of Detonations in Hydrogen-Air and Methane-Air Mixtures", *Eighteenth Symposium (International) on Combustion*, The Combustion Institute (1981), 1641–1649.

[17] Taki, S. and Fujiwara, T., "Numerical Analysis of Two Dimensional Nonsteady Detonations," *AIAA J.* **16** (1978), 73–77.

[18] Korobeinikov, V. P., Levin, V. V. Markov and Chernyi, G. G.; *Astronautica Acta* **17**, 529 (1972).

[19] Bourlioux, A. and Majda, A. J., "Theoretical and Numerical Structure for Unstable Two-dimensional Detonations," *Combustion and Flams* 90: 211-229 (1992).

[20] Harten, A., "On High Order Accurate Interpolation for Non-Oscillatory Shock Capturing Schemes," *IMA Program on Continuum Physics and Its Applications,* 1984-85, pp. 72-105.

[21] Shu, C. W. and Osher, S., " Efficient Implementation of Essentially Nonoscillatory Shock Capturing Schemes," J. Compt. Phys., **77** (1988), 439-471.

[22] Cai, W., Oh, W. H., Zhu, Y. L.," Direct Numerical Calculations of Neutral Stability Curve of One-Dimensional Detonation Waves," Submitted to *SIAM J. Sci. Stat. Computing*

[23] Zhu, Y. L., Zhong, X. C., Chen, B. M., and Zhang, Z. M., *Difference Methods for Initial Boundary Value Problems and Flow around Bodies,*, Springer-Verlag, Heidelberg and Science Press, Beijing, 1988.

[24] Gottlieb, D., Gunzburger, M., Turkel, E., On Numerical Boundary Treatment for Hyperbolic Systems, SIAM J. Numer. Anal. **19**, (1982), 671-697.

[25] Zannetti, L. and Colasurdo, G, *AIAA J.* **19**, 758 (1984)

[26] Kopriva, D., A., "Multi-domain Spectral Solution of Euler Gas-Dynamics Equations," *J. Compt. Phys.* **96** (1991) 428-450.

[27] Hyman, J. M. 1984, "Numerical Methods for Tracking Interfaces," *Physica* 12D: 396-407

[28] P. Roe, "Approximate Riemann Solvers, Parameter Vectors, and Difference Schemes, " *J. Compt. Phys.*, V. 43 (1981), pp. 357-372.

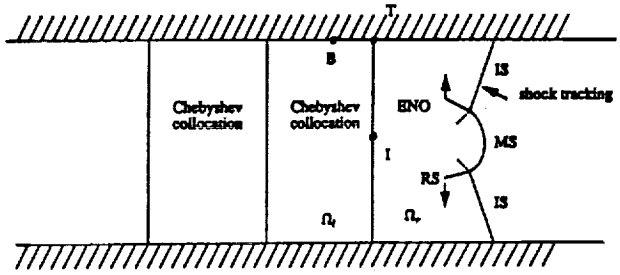

(a)

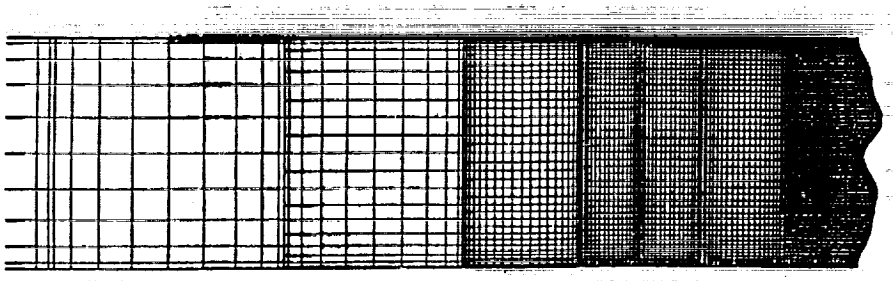

(b)

Figure 1 (a) Multidomain set-up for the hybrid numerical scheme for detonation waves; (b) Mesh structures for 2-D detonation waves

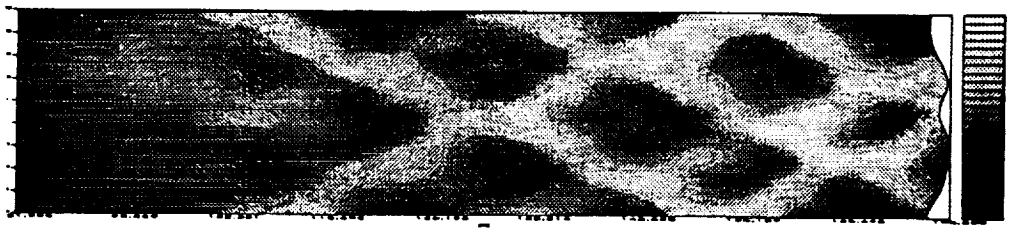

(a)

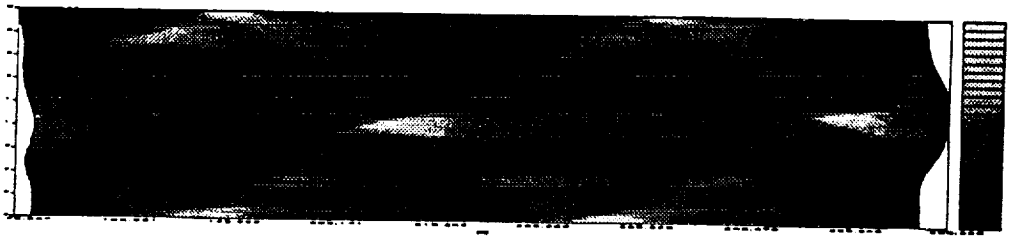

(b)

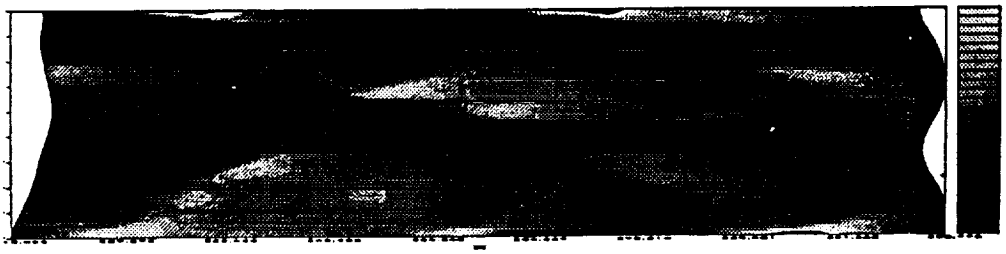

(c)

Figure 2 Cellular pattern for $Q = 50, E = 50, f = 1.6$ with different smoothings on the detonation front (a) Smoothing I, II and III, (b) Smoothing II, III; (c) Smoothing III only.

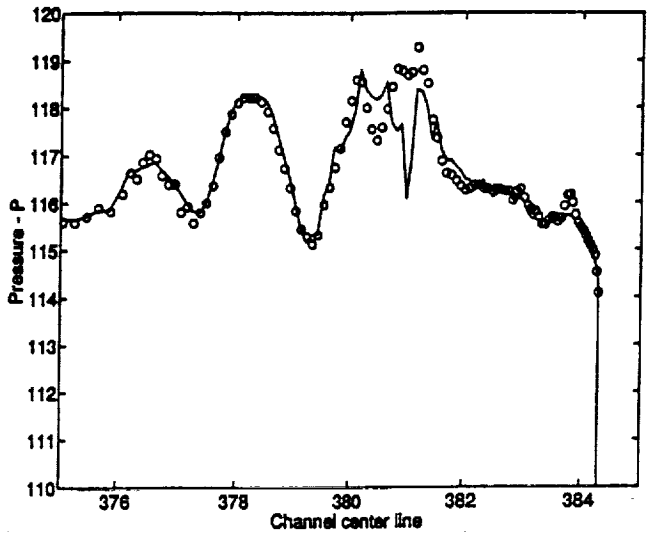

Figure 3 Pressures along the center of channel obtained by time splitting (0) and third order Runge-kutta (-).

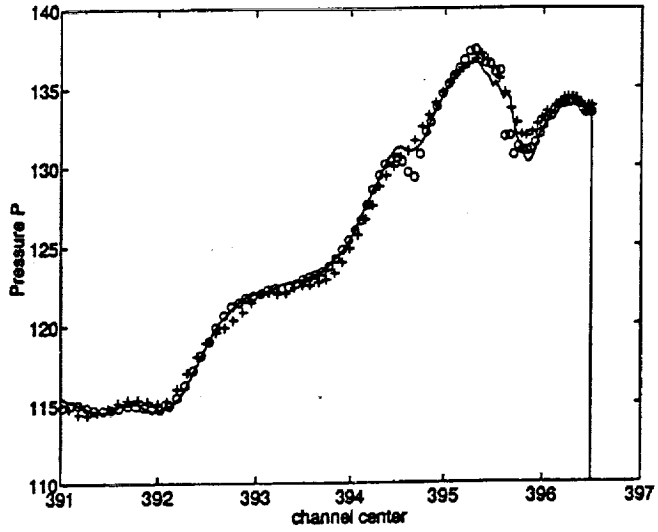

Figure 4 Mesh convergence studies: Pressure along the center of channel with three meshes (-) 20 points per ℓ^*, (o) 15 points per ℓ^*, (+) 10 points per ℓ^*.

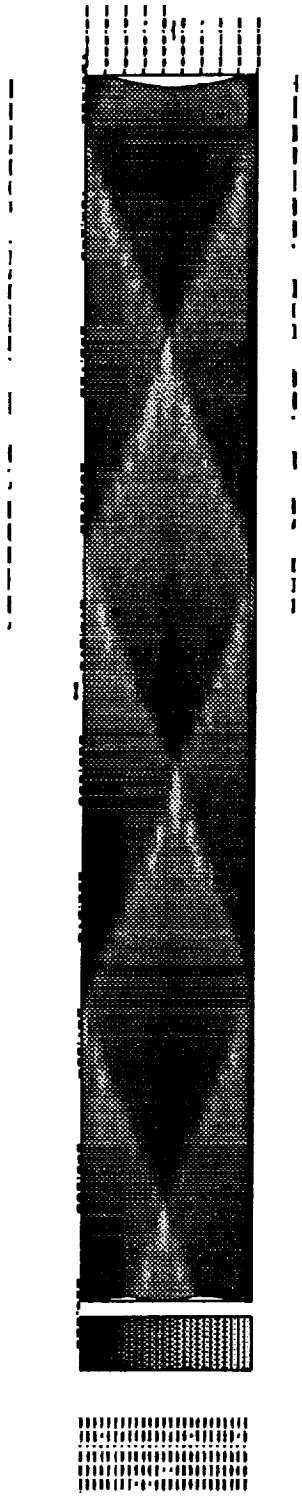

Figure 5 Case I, $Q = 10, E = 50, f = 1.2, W = 10$ (a) one cell pattern, (b) five snapshots of pressure, temperature, vorticity, mass fraction of reactant (from top to bottom) at $T = 30.5t^*, 31.5t^*, 32.5t^*, 33.5t^*, 34.5t^*$, (c) sketch of the interaction of the triple points.

Figure 5b

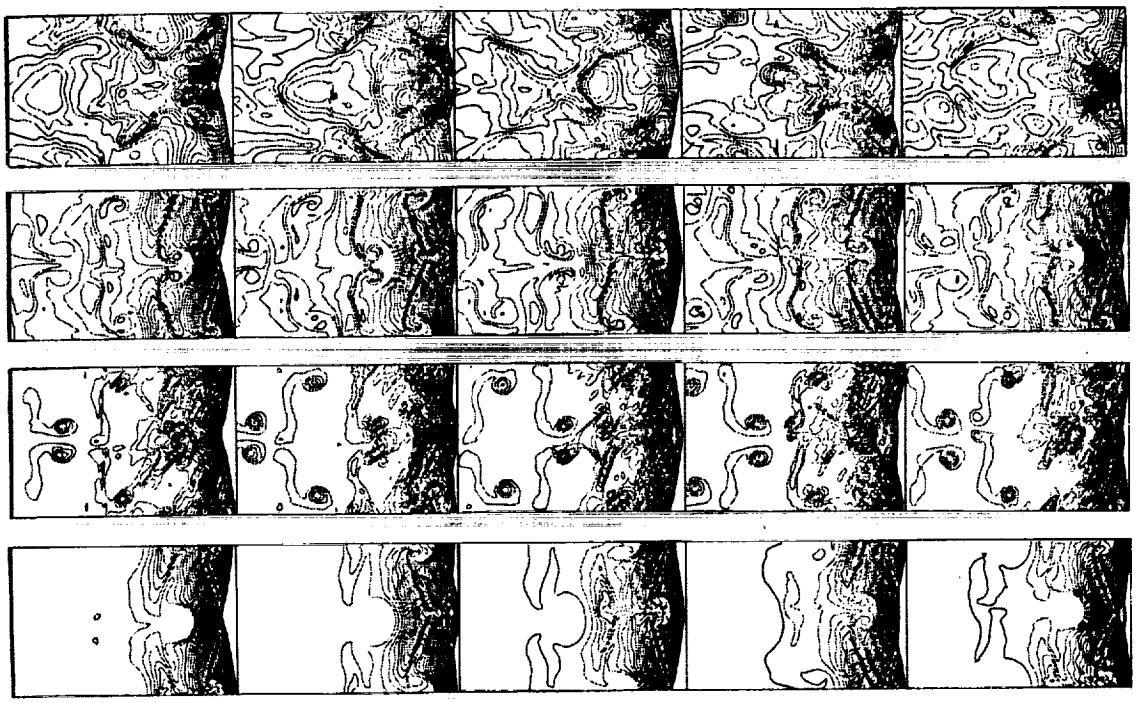

Figure 5c

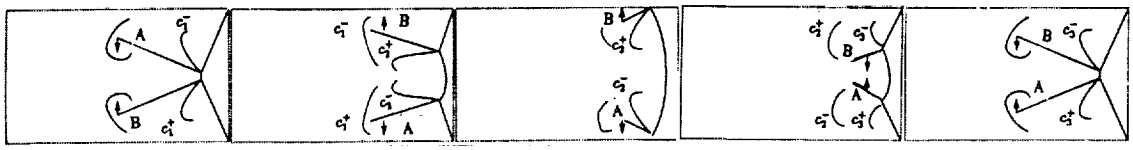

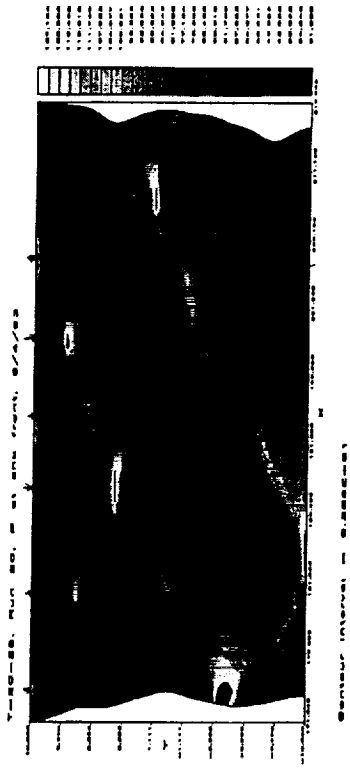

Figure 6 Case II, $Q = 50, E = 50, f = 1.6, W = 20$ (a) two cell pattern, (b) six snapshots of pressure, temperature, vorticity, mass fraction of reactant (from top to bottom) at $T = 20.25t^*, 21.5t^*, 22t^*, 22.5t^*, 23t^*, 23.5t^*$. (c) Tracks of the triple points.

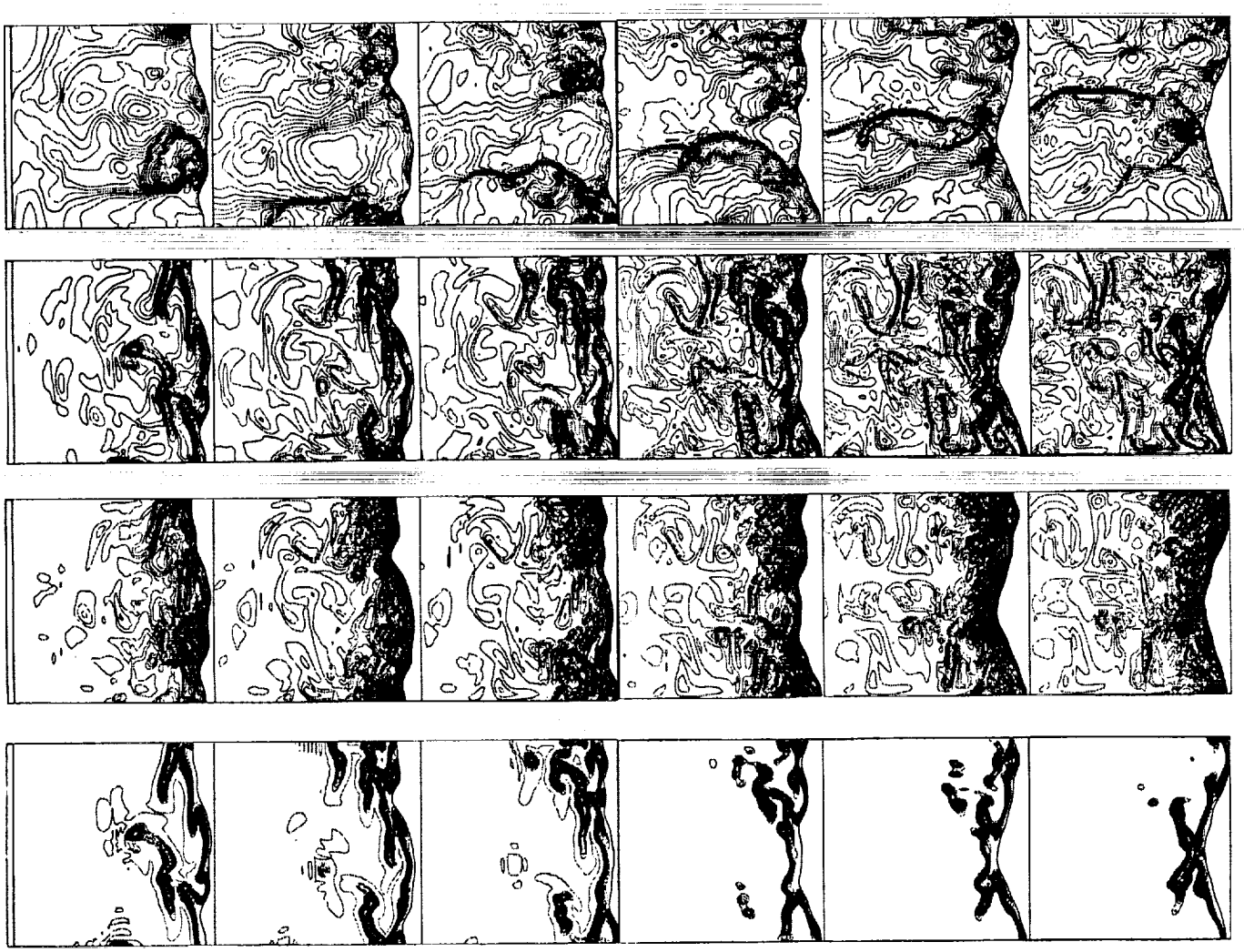

Figure 6b

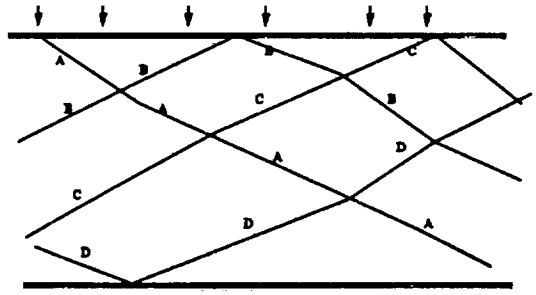

Figure 6c

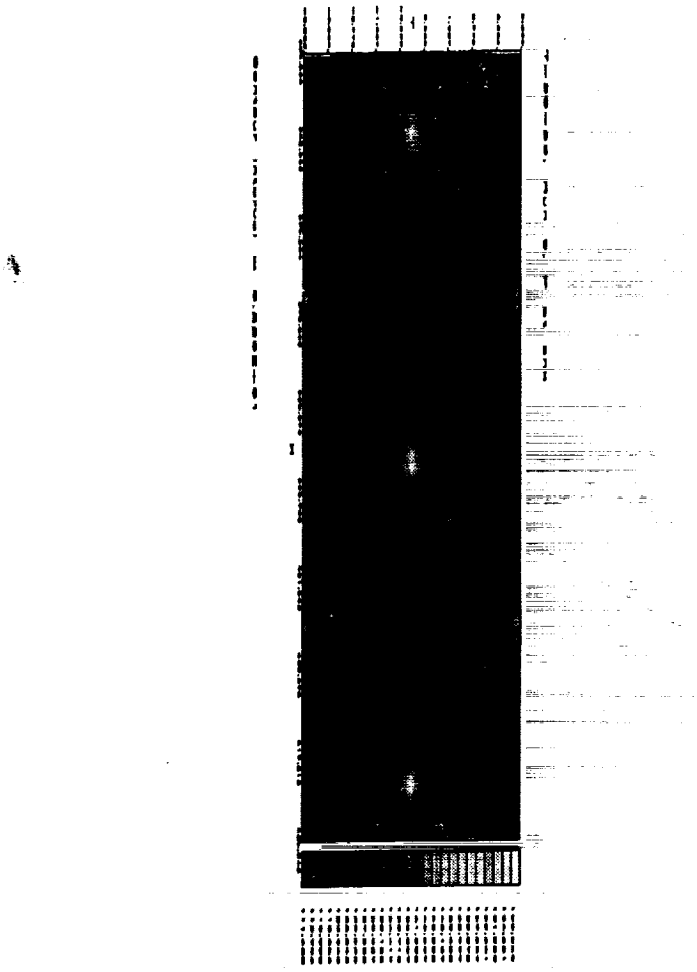

Figure 7 Case III, $Q = 50, E = 50, f = 3, W = 10$ (a) one cell pattern, (b) six snapshots of pressure, temperature, vorticity, mass fraction of reactant (from top to bottom) at $T = 33t^*, 33.5t^*, 34t^*, 34.5t^*, 35t^*, 35.5t^*$.

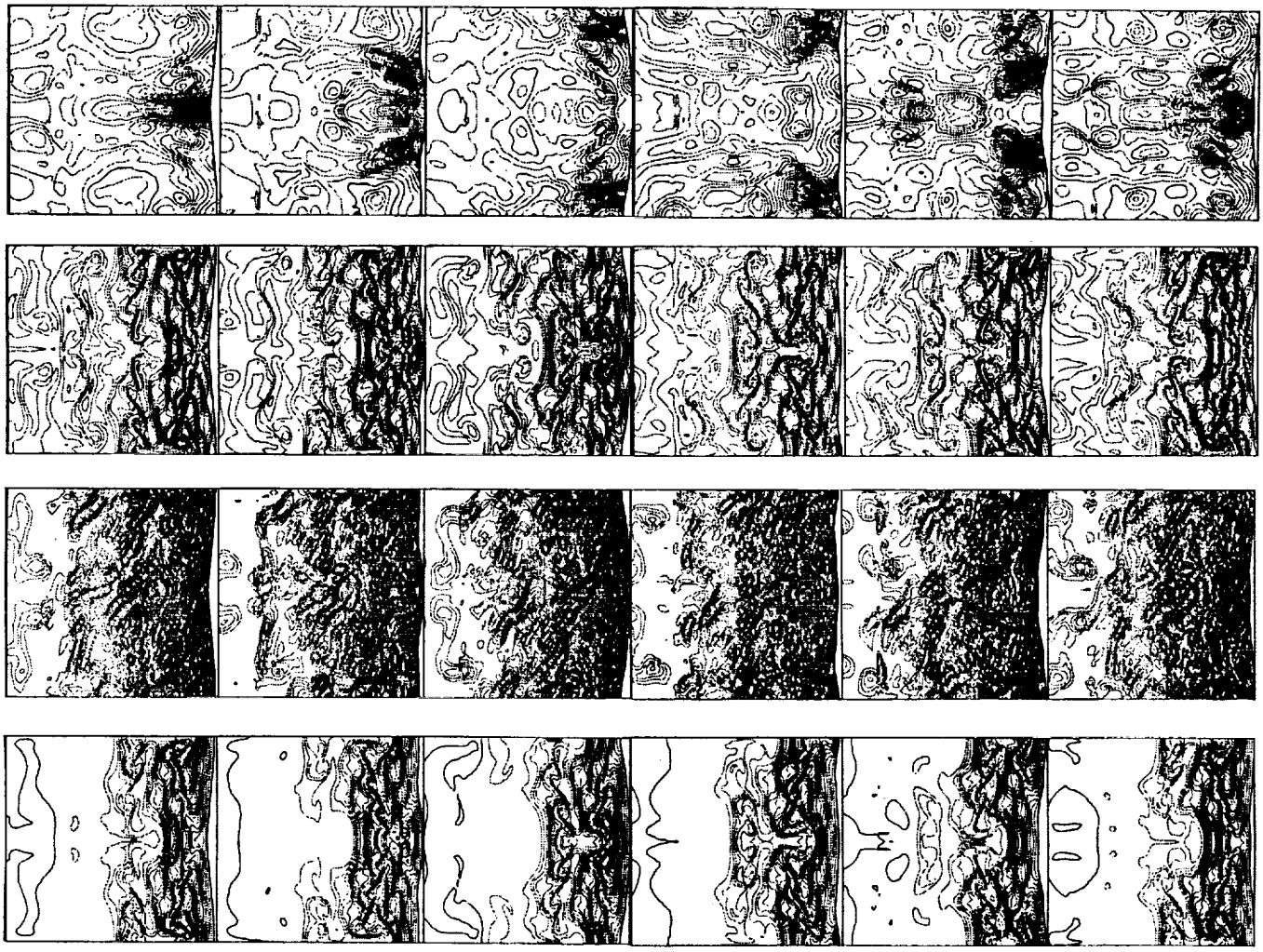

Figure 7b

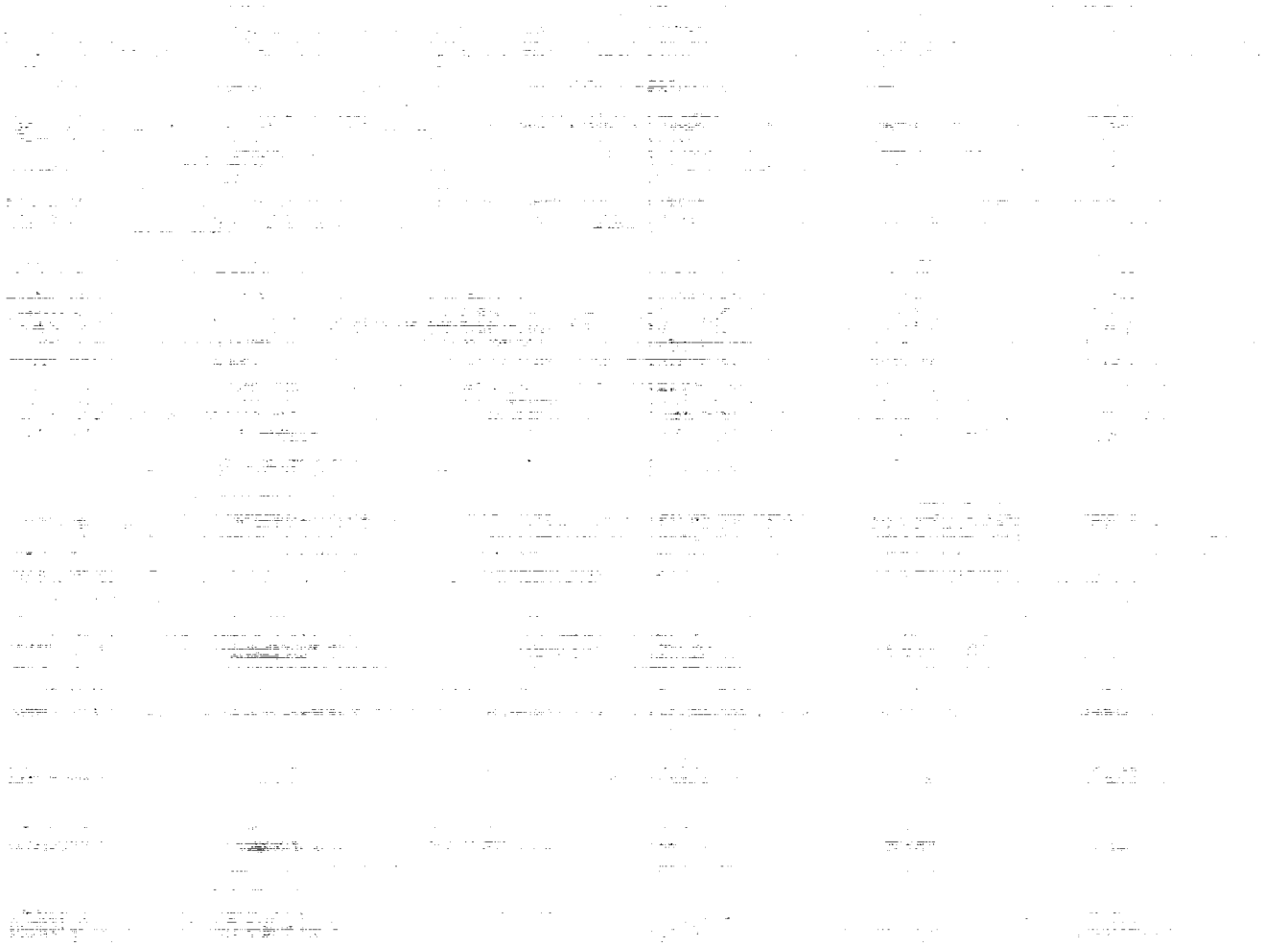

REPORT DOCUMENTATION PAGE

Form Approved
OMB No 0704-0188

1. AGENCY USE ONLY (Leave blank)	2. REPORT DATE	3. REPORT TYPE AND DATES COVERED
	July 1993	Contractor Report

4. TITLE AND SUBTITLE

HIGH ORDER HYBRID NUMERICAL SIMULATIONS OF TWO DIMENSIONAL DETONATION WAVES

5. FUNDING NUMBERS

C NAS1-19480

WU 505-90-52-01

6. AUTHOR(S)

Wei Cai

7. PERFORMING ORGANIZATION NAME(S) AND ADDRESS(ES)

Institute for Computer Applications in Science and Engineering
Mail Stop 132C, NASA Langley Research Center
Hampton, VA 23681-0001

8. PERFORMING ORGANIZATION REPORT NUMBER

ICASE Report No. 93-47

9. SPONSORING/MONITORING AGENCY NAME(S) AND ADDRESS(ES)

National Aeronautics and Space Administration
Langley Research Center
Hampton, VA 23681-0001

10. SPONSORING/MONITORING AGENCY REPORT NUMBER

NASA CR-191506
ICASE Report No. 93-47

11. SUPPLEMENTARY NOTES

To be submitted to AIAA J.

Langley Technical Monitor: Michael F. Card
Final Report

12a. DISTRIBUTION/AVAILABILITY STATEMENT

Unclassified - Unlimited

Subject Category 64

12b. DISTRIBUTION CODE

13. ABSTRACT *(Maximum 200 words)*

In order to study multi-dimensional unstable detonation waves, we have developed a high order numerical scheme suitable for calculating the detailed transverse wave structures of multidimensional detonation waves. The numerical algorithm uses a multi-domain approach so different numerical techniques can be applied for different components of detonation waves. The detonation waves are assumed to undergo an irreversible, unimolecular reaction $A \rightarrow B$. Several cases of unstable two dimensional detonation waves are simulated and detailed transverse wave interactions are documented. The numerical results show the importance of resolving the detonation front without excessive numerical viscosity in order to obtain the correct cellular patterns.

14. SUBJECT TERMS

detonation waves, instability, cellular pattern

15. NUMBER OF PAGES

41

16. PRICE CODE

A03

17. SECURITY CLASSIFICATION OF REPORT	18. SECURITY CLASSIFICATION OF THIS PAGE	19. SECURITY CLASSIFICATION OF ABSTRACT	20. LIMITATION OF ABSTRACT
Unclassified	Unclassified		

NSN 7540-01-280-5500

Standard Form 298 (Rev. 2-89)
Prescribed by ANSI Std Z39-18
298-102

☆U.S. GOVERNMENT PRINTING OFFICE: 1993 - 728-064/86045